Biomaterials 32 (2011) 2725–2733

Contents lists available at ScienceDirect

Biomaterials

journal homepage: www.elsevier.com/locate/biomaterials

Elasticity boundary conditions required for cell mechanotaxis on microelastically-patterned gels

Takahito Kawano, Satoru Kidoaki*

Division of Biomolecular Chemistry, Institute for Materials Chemistry and Engineering, Kyushu University, Fukuoka 819-0395, Japan

ARTICLE INFO

Article history:
Received 29 October 2010
Accepted 5 January 2011
Available online 26 January 2011

Keywords:
Mechanotaxis
Durotaxis
Cell migration
Styrenated gelatin
Microelasticity patterning

ABSTRACT

Directional cell migration induced by a mechanical gradient on a substrate surface toward a harder region, so-called mechanotaxis or durotaxis, has recently drawn attention not only in the field of mechanobiology but also for possible cell manipulation in biomedical engineering. Before we can use mechanotaxis to control cell migration on a biomaterial surface, quantitative design criteria for a microelasticity gradient should be established. To clarify the conditions required to induce mechanotaxis, the effects of a microelasticity boundary on cell culture hydrogels have been systematically assessed with regard to fibroblast migration based on a custom-built reduction projection-type photolithographic microelasticity patterning system with elasticity-tunable photocurable styrenated gelatins, which is a thoroughly-improved system of our previous simple photomasking method [41]. As a result, the conditions required to induce mechanotaxis were found to include a certain threshold jump in elasticity (30–40 kPa) and a sufficiently narrow width of the elasticity boundary (50 μm) comparable to a single cell's adhered area, i.e., a sufficiently high gradient strength (30–40 kPa/50 μm in our gelatinous gel system). A significant asymmetric distribution of the number and size of focal adhesions across the elasticity boundary was confirmed to be one of the driving factors of mechanotaxis by indirect immunofluorescence microscopy, and mechanistic considerations in the design criteria are discussed.

1. Introduction

Organized cell migration *in vivo* underlies various activities of living tissue, including morphogenetic processes ranging from gastrulation to the development of a nervous system [1], inflammation processes starting from the migration of leukocytes into an area of insult [2,3], and wound-healing processes that involve the migration of fibroblasts and vascular endothelial cells [4]. On the other hand, disordered cell migration can cause diseased tissue reactions such as those seen in tumor metastasis [5], where tumor cells migrate from the initial tumor mass into the circulatory system and spread to new sites. Since the appropriate control of cell migration should make it possible to regulate such physiological and pathological processes, the active control of cell migration has been an important issue in the fields of medicine and bioengineering [6–11]. For this purpose, the manipulation of taxis behavior, i.e., external-stimulant-induced directional cell movement, has been investigated in terms of the manner of application of an external stimulant, which typically consists of liquid-soluble chemoattractants [12,13], surface-fixable haptoattractants [14–16], etc. Especially, the engineering of biomaterial surfaces, 3D matrices and scaffolds to control the migration of cells in which they reside is expected to be a key technology for the development of a functional platform for biomedical cell manipulation as well as for the systematic investigation of the mechanisms that underlie cell motility [17–25].

For the development of such functional biomaterials, it is important that we learn to control substrate-induced taxis behavior, which has been a focus of research in terms of the effects of the surface topography, chemistry and mechanics, which include contact guidance taxis induced by the substrate topography [26,27], haptotaxis induced by surface-fixed haptoattractants [28,29] and mechanotaxis induced by a surface-mechanical gradient [30], respectively. Although many previous studies have examined the control of contact guidance and haptotaxis, there have been insufficient studies on the application of mechanotaxis for biomaterial engineering, since conditions for the systematic distribution of surface microelasticity to manipulate mechanotaxis have not been fully established.

Mechanotaxis was first observed on a mechanical gradient surface with an elasticity boundary between juxtaposed hard and soft hydrogels as directional cell movement toward the harder region (hence the original term "durotaxis") [30], and the importance of a steep and discontinuous boundary was suggested. This

* Corresponding author. Tel.: +81 92 802 2507; fax: +81 92 802 2509.
E-mail address: kidoaki@ms.ifoc.kyushu-u.ac.jp (S. Kidoaki).

0142-9612/$ – see front matter © 2011 Elsevier Ltd. All rights reserved.
doi:10.1016/j.biomaterials.2011.01.009

interesting taxis behavior has recently drawn attention not only in the field of mechanobiology but also for possible application to cell manipulation in biomedical engineering. While some groups have since tried to prepare cell-adhesive hydrogels with a microelasticity gradient or patterns [31–41], the systematic and precise preparation of steep and discontinuous elasticity boundaries with both smooth topographical continuity and uniform cell adhesiveness across the boundary have not yet been realized due to technical difficulties. The elasticity boundary conditions, and particularly the elasticity jump height and gradient width, needed to induce mechanotaxis have remained unclear.

In our previous study, we developed a simple system of visible light-based photolithographic microelasticity patterning of elasticity-tunable photocurable gelatinous gels, and observed mechanotaxis behaviors on it [41]. Due to the quasi-contact manner of photomasking employed in the system, design of elasticity boundary condition was not so precise that the systematic investigation of the boundary conditions could not be performed. Therefore in the present study, we sought to establish quantitative precise design criteria for the elasticity boundary conditions needed to induce mechanotaxis by introducing a custom-built equipment of reduction projection-type photolithographic microelasticity pattering. By using the new system, we prepared microelasticity-patterned gels with square hard domains within a softer surrounding gel. The jump in elasticity across the boundary was adjusted by regulating the photo-gelation conditions by varying the photoirradiation power and duration, and the boundary width was regulated by controlling the focus in reduction-projected images of photomasks. The effects of the elasticity jump and boundary width were assessed systematically. As a result, the conditions required to induce mechanotaxis were found to be a jump in elasticity of a certain threshold magnitude (30–40 kPa) and a sufficiently narrow width of the elasticity boundary (50 μm), comparable to the adhesion area of a single cell. Based on the precise and systematic fabrication of the microelasticity boundary, the generation of cell polarity across the boundary was confirmed by the indirect immunofluorescence microscopic observation of an asymmetric distribution in the amount and size of focal adhesions (FAs). Mechanistic considerations for the design criteria required to induce mechanotaxis are discussed.

2. Materials and methods

2.1. Styrenated gelatin

Photo-crosslinkable styrenated gelatin (StG) was used for photolithographic microelastic patterning of the gelatinous gel, which was synthesized by the condensation reaction between 4-vinyl benzoic acid (VBA; Wako Pure Chemical Industries, Ltd., Osaka, Japan) and amine groups in the lysine and hydroxylysine residues of gelatin (derived from beef bones, Wako) mediated by water-soluble carbodiimide (WSC; Watanabe Chemical Industries, Ltd, Hiroshima, Japan) [42]. Gelatin, VBA, and WSC were dissolved in phosphate-buffered saline (PBS) in a molar equivalent ratio of 1 (amine groups of gelatin):10 (VBA):10 (WSC). The solution was then allowed to stand at pH 8.0 for 2 days, and the resulting gelatin was freeze-dried after 3 days of dialysis to remove non-reacted species. In this study, the degree of derivatization (DD) of styrene groups on StG as evaluated by UV absorption at 265 nm was 85–95%.

2.2. Preparation of photocurable sol solution

A photocurable sol solution of StG was prepared as follows: (1) StG (30 wt%) and sulfonyl camphorquinone (SCQ; Toronto Research Chemicals, ON, Canada; 1.5 wt% of gelatin) were dissolved in PBS. (2) The mixed solution was subjected to high-speed centrifugation (MX-301; TOMY, Tokyo, Japan) at 14,000 rpm (17,800 × g) for 1 h to spin-down colloidal coagulations, and the deposit was removed. (3) The clear sol solution was mildly aspirated to exclude dissolved oxygen, conditioned for 10 min using a deforming agitator (MX-201; THINKY, Tokyo, Japan), and stored at −20 °C. The sol solution was warmed at 45 °C prior to use for photolithography. Since the photocuring efficiency of the StG sol solution is sensitively reduced depending on the duration of storage, the sol solution was either used within one week or discarded.

2.3. Preparation of supporting glass substrates to fix gel samples

Vinyl-silanized glass substrates (vinyl-glass) were prepared to chemically fix the photocured StG gels according to the following procedures: (1) glass substrates (0.12–0.17 mm thickness, 15-mm diameter; Matsunami Glass Ind., Ltd., Osaka, Japan) were immersed in 80 °C piranha solution (conc. H_2SO_4: 30% H_2O_2 = 7:3) for 1 h; (2) After sequential rinsing with distilled water (DDW), acetone and toluene, the glass substrates were immersed in a 5% (v/v) toluene solution of vinyltrimethoxysilane (Tokyo Chemical Industry Co. Ltd., Tokyo, Japan), and shaken for 18 h at room temperature. (3) After sequential rinsing with toluene, acetone, ethanol, and DDW, the glass substrates were dried at 115 °C for 10 min in air.

2.4. Photolithographic microelasticity patterning of gelatinous gel

Photolithographic microelasticity patterning of the StG sol was performed as follows: 30 μl of StG sol solution were spread between vinyl-glass and a normal glass substrate coated with poly(N-isopropylacrylamide) (PNIPAAm, Sigma Aldrich Co. MO, USA), and the sample was placed on a hot plate at 45 °C. PNIPAAm was used to ensure that photocured StG gel could be easily removed from the normal glass substrate by treating it with an aqueous solution below the lower critical solution temperature (LCST). First, the soft base gel was prepared by irradiation of the entire sample with visible light (100 mW/cm^2 at 514 nm, 20 s) through the back of the vinyl-glass. Next, a hard domain was prepared by subsequent local irradiation (120 mW/cm^2 at 514 nm, 5–30 s) of the soft base gel through a micropatterned photomask using a custom-designed reduction projection-type photolithographic system, as shown schematically in Scheme 1. In this system, a 2× objective lens (NA 0.1, Nikon Corporation, Tokyo, Japan) and a metal halide light source (MME-250; Moritex, Tokyo, Japan) were used. Light intensity was measured using a laser power meter (HP-3; Pneum Co., Ltd. Saitama, Japan). To control the sharpness of the elasticity gradient, the position of the focal plane of the projected photomask pattern was regulated by changing the z-position of the objective lens within the range of 1–3 mm. Finally, the produced gels were detached from the PNIPAAm-coated normal glass substrate and thoroughly washed in PBS at room temperature to completely remove the adsorbed PNIPAAm.

2.5. Measurement of the surface elasticity distribution around the elasticity boundary

The surface elasticity of the photocured StG gel was determined by nano-indentation analysis using atomic force microscopy (AFM). Force-indentation (f–i) curves were measured for the gel surface using AFM (NVB100; Olympus Optical Co.

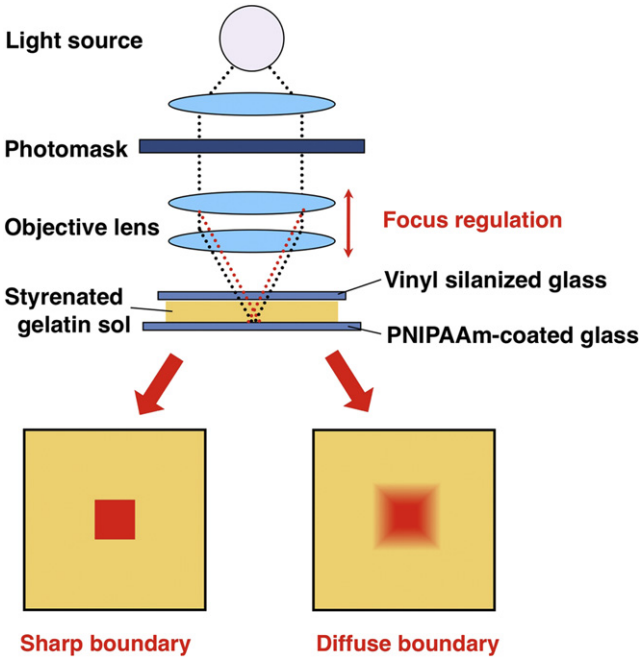

Scheme 1. Schematic representation of the reduction projection-type photolithographic microelasticity patterning of styrenated gelatin gel. The resulting gel sample is attached to the top of vinyl-silanized glass, and photomask patterns are copied on the bottom of the gel surface covered with PNIPAAm-coated glass. The boundary conditions of the elasticity gradient can be controlled by raising the lens position and focusing out from the gel surface.

Ltd., Tokyo, Japan; AFM controller & software, Nanoscope IIIa; Veeco Instruments, CA, USA) along with a commercial silicon-nitride cantilever with a pyramidal tip and a nominal spring constant of 0.02 N/m (OMCL-TR400PSAHW, Olympus Optical Co. Ltd. Tokyo, Japan) in PBS. The frequency of the tip approach/retract cycle was chosen to be 1 Hz to minimize noise fluctuation within a single *f*–*d* curve. Young's moduli of the surface were evaluated from *f*–*i* curves by nonlinear least-squares fitting to the Hertz model in the case of a conical indenter [Eq. (1)] (semi-vertical angle α: 18°, Poisson ratio μ: 0.5) [43–45].

$$F = \frac{2E}{\pi \tan\alpha(1-\mu^2)}\delta^2 \quad (1)$$

The distribution of Young's moduli around the elasticity boundary was obtained through manual force-volume measurement with a resolution of 50 μm.

2.6. Cell culture

A mouse fibroblast cell line (3T3-Swiss albino) purchased from Dainippon Pharmaceutical Co. Ltd. (Osaka, Japan) was cultured in Dulbecco's modified Eagle's medium (DMEM; Gibco BRL, Grand Island, NY, USA) supplemented with 10% fetal bovine serum (FBS; Gibco BRL), 3.5 g/l glucose, 2 mM L-glutamine, 100 units/ml penicillin, and 100 μg/μl streptomycin. Cells were maintained on tissue culture polystyrene dishes at 37 °C under 5% CO_2 in a humidified incubator.

2.7. Time-lapse observation of cell migration

The migratory behavior of cells on the microelasticity-patterned gel surface was monitored using a time-lapse image-capturing camera (VB-6000; Keyence Corporation, Osaka, Japan) connected to a phase-contrast microscope (TE300; Nikon) with a temperature- and humidity-controllable cell chamber. Prior to the time-lapse observation, cells were seeded at a density of 1.5×10^3 cells/cm^2 on the gel sample and cultured with DMEM containing 10% FBS under 5% CO_2 for 8 h. DMEM was then replaced by L15 (Gibco BRL) containing 10% FBS to adapt the cultured cells to the long observation period without needing to regulate the CO_2 concentration in the cell chamber. Images of cells were captured every 15 min for 20 h. The coordinates of 20 isolated cells and the migratory track were measured using ImageJ software.

2.8. Confocal microscopic observation

The amount of fibronectin adsorbed onto the microelasticity-patterned gel surface (a), the topographical features of the surfaces (b), and the distribution of focal adhesion (c) were characterized using a confocal laser scanning microscope (LSM510META, Carl Zeiss, Oberkochen, Germany): (a) Alexa Fluor 488-conjugated fibronectin (Alexa-fibronectin) was adsorbed onto the gels for 24 h. The fluorescence intensity of adsorbed Alexa-fibronectin on the top of the gel surface was measured for a confocal slice image of the surface. (b) For the analysis of surface topography, the gels were adsorbed and stained with fluorescein-conjugated albumin, and confocal cross-sectional observation was performed. (c) For characterization of the distribution of focal adhesions formed on the gel surface, cells were cultured on the gel samples for 24 h, fixed with 4% formaldehyde, blocked in 10% donkey serum, and permeabilized with 0.1% Triton-X 100 at room temperature for 1 h. Cells were incubated with anti-paxillin (Santa Cruz Biotechnology, CA, USA, diluted 1:200) for 1 h, and then incubated in Alexa488-anti rabbit IgG (Invitrogen, CA, USA, diluted 1:1000) and rhodamine-phalloidin (Cytoskeleton, CO, USA) for 1 h. The samples were mounted on cover glass and observed with a 63× oil-immersion objective lens.

2.9. Image analysis for characterization of the distribution of focal adhesions

Confocal microscopic images of focal adhesions visualized by indirect immunofluorescence of vinculin were quantitatively characterized by the following protocol using MetaMorph version. 7.6 image analysis software (Molecular Devices, Inc., CA., USA.); raw 8-bit images were treated by (1) flattening the background to reduce significant noise, (2) thresholding over a certain lower criteria (12 as gray-scale) to offset the constant background level, and (3) Integrated Morphometric Analysis to measure the area, position and long-axis length of all objects except those smaller than 3 pixels. These treatments were applied to the confocal image obtained under the standardized constant parameters for confocal microscopy to enable the relative quantitative comparison among different images.

3. Results

3.1. Preparation of elasticity boundaries with different gradient conditions

To establish quantitative criteria for an elasticity gradient to induce cell mechanotaxis, microelasticity-patterned gelatinous gels with different boundary conditions for the elasticity gradient were prepared by a photolithographic technique. Since the spatial distribution of the degree of crosslinking in hydrogels of photocurable styrenated gelatin can be controlled by locally regulating the power, duration and position of photoirradiation, it is possible to systematically prepare microelasticity-patterned gels with different elasticity gradient boundaries. To assess the effects of the magnitude of the jump in elasticity and the width of the boundary, the duration of photoirradiation and the focus of the projected patterns of the photomask were controlled, respectively, as described in the legend for Fig. 1.

Fig. 1 shows microelasticity-patterned gels with five different boundary conditions for the 400 μm square hard domains. For Gels A, B, and C, elasticity jumps of 2.7 ± 0.9 kPa, 21.3 ± 1.6 kPa and 42.1 ± 18.1 kPa from the softer 1.2 ± 0.5 kPa base were successfully achieved within the 50 μm gradient width. The durations of photoirradiation for the hard domain were 5, 10 and 30 s, respectively, under the fixed-focus setting in which the lens (2×; focus depth: 1.8 mm) was positioned 1 mm above the central focal plane of the gel surface on PNIPAAm-coated glass (Scheme 1). This somewhat irregular focal condition was purposely set to avoid significant topographic turbulence between the soft and hard regions, which is inevitably caused by swelling discordance across the boundary (data shown in Fig. 2, explained in detail in the next section). Gels A, B, and C were used to determine the effect of the magnitude of the elasticity jump on the efficiency of the induction of mechanotaxis under a fixed boundary width. On the other hand, in Gels C, D and E, the initial jumps in elasticity from the softer base region were all ca. 40 kPa (44.2 ± 7.3 kPa), due to irradiation of the hard domain for 30 s, while the width of the boundary was 50, 150, or 200 μm, which was achieved by setting the focal position at 1, 2, or 3 mm above the gel surface, respectively. This series of samples was used to evaluate the effect of the width of the elasticity gradient on mechanotaxis behavior.

3.2. Surface topography and adsorption of fibronectin around the microelasticity boundaries

In general, cell motility should be affected by the surface topographic features and the density gradient of surface biochemical factors to determine cell adhesivity. To solely investigate the mechanical effect of the microelasticity boundary on mechanotaxis behavior, the contributions of these two factors should be excluded. These two factors were characterized as follows.

First, to assess the surface topography of the prepared microelasticity gradient boundaries, the gels were stained by the adsorption of fluorescein-labeled albumin, and cross-sectional observation was performed by confocal microscopy. As shown in Fig. 2a, while the soft regions on the right side were significantly swollen by about 20 μm compared with the hard regions on the left side, the regions of Gels A, B and C were smoothly connected across the elasticity boundary, which reflects a similar topography. These three conditions did not exhibit significant differences in surface topography, which suggests that we can examine the mechanical effect of an elasticity gradient on cell motility on these gels separate from any topographic issues. Note that this smooth topographic transition between adjacent hard and soft regions was achieved by regulating the photolithographic focus. When we focused on the outermost gel surface, hill-and-valley features in the area around the boundary were produced and the smooth transition between adjacent regions was disturbed (data not shown). To exclude the contribution from such a topographic effect, we discarded this condition of focusing, and adopted a 1 mm above focal condition.

Next, to check the adsorption of cell-adhesive proteins on regions of different elasticity, we measured the amount of adsorbed

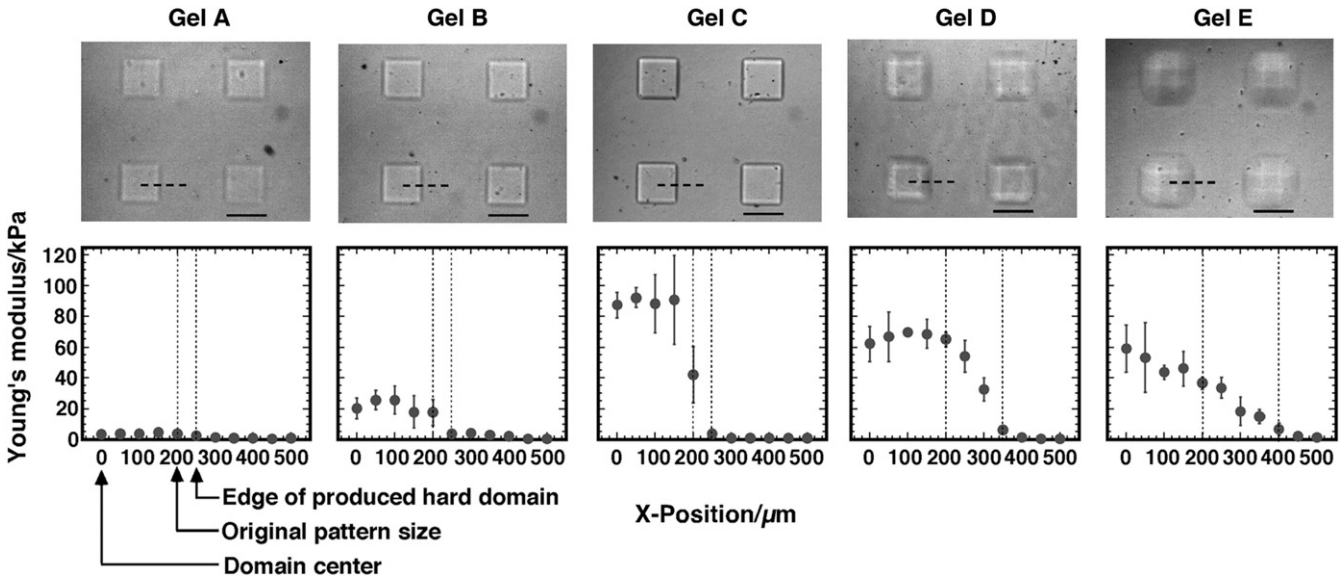

Fig. 1. Micropatterned square hard domains with elasticity gradients with different boundary conditions. Upper photos: phase-contrast microscopic images of each gel. Lower graphs show the distribution of Young's modulus around the boundary measured along the broken line indicated in the upper photos. Scale bar: 400 μm. Photoirradiation duration, focus setting: Gel A; 5 s, 1 mm above. Gel B; 10 s, 1 mm above. Gel C; 30 s, 1 mm above. Gel D; 30 s, 2 mm above. Gel E; 30 s, 3 mm above. The edge of the domain was defined as the position where Young's modulus significantly increased from the soft plateau region.

fibronectin on hard (90 kPa) and soft (2 kPa) regions of Gel C, which had the largest jump in elasticity among the prepared gels. Alexa 488-labeled fibronectin was absorbed on the gel surface for 24 h and the fluorescence intensity profiles on the top surface layer (10 μm-thick) of the hard and soft regions was observed by confocal microscopy (Fig. 2b). The fluorescence intensity was almost the same in the hard and soft regions, indicating that they had almost the same amounts of adsorbed fibronectin. Therefore, we can exclude the possibility of haptotactic motility induced by a density gradient of adsorbed cell-adhesion proteins in the following experiment.

3.3. Cell migration around elasticity boundaries with different gradient conditions

To determine the conditions of a microelasticity gradient needed to induce cell mechanotaxis, we observed cell migration on the above-prepared microelastic-patterned gels with different elasticity gradient conditions. Fibroblast 3T3 cells were seeded on gels at a low seeding density to exclude the contribution of cell–cell interactions, which disturb the standard mechanics of cell-substrate interactions. Fig. 3 shows the observed trajectories of cells located near the boundaries on each gel. In each plot, the results of three runs under time-lapse observation are superimposed, and the positions of the outer edge of the square hard domain were determined from the data on the elasticity distribution measured in Fig. 1. The square domains in Gels A, B, C, D, and E were 500, 500, 500, 700 and 800 μm on a side, respectively. Among these five gels, biased cell migration toward the harder region was only observed on Gel C, while the other gels did not show clear biased cell trajectories (also see the Supplemental video data, file names: Gel A, Gel C, and Gel E).

Supplementary data related to this article can be found online at doi:10.1016/j.biomaterials.2011.01.009.

To more closely examine the biased trends toward the harder region, the observed raw trajectories were presented in a different format (Fig. 4a) by setting the starting position of each cell trajectory as the origin of the graph, where the elasticity boundary of each domain is the *Y*-axis. In this new format, the positive *Y*-direction was defined as the counterclockwise direction of the domain's boundary, and the positions relative to the nearest boundary were re-plotted for each cell. For example, if a cell migrated across the domain's boundary from outer hard region into soft domain, the trace would be appeared in the left side, i.e., minus *X*-direction. Inversely, it migrated toward hard region, the trace would be described in the right side, i.e., plus *X*-direction. Near the elasticity boundaries on Gel A (ca. 3 kPa jump) and Gel B (ca. 20 kPa jump) with a 50 μm-wide gradient, the *X*–*Y* trajectory showed an almost isotropic distribution, and the time-course trajectories in the *X*- and *Y*-directions were dispersed randomly. Biased trajectories toward the harder square regions from the softer base region, i.e., minus *X*-direction, were only observed on Gel C (ca. 40 kPa jump with a 50 μm-wide gradient), i.e., marked mechanotaxis was induced. Since the elasticity gradient became less sharp from Gel C (50 μm-wide), to D (150 μm-wide), to E (300 μm-wide) under almost the same jump in elasticity (ca. 40 kPa), both the *X*- and *Y*-trajectories and the time-course trajectories showed a progressively random distribution. In addition, as seen in Fig. 4b, the ensemble-averaged time-course *X*-trajectories clearly established a time-dependent biased motility towards a harder region only on Gel C, while movement on the other gels was almost random.

These results showed that directional motility toward a harder region occurred with a boundary with a jump in elasticity of 40 kPa over a 50 μm-wide gradient, which suggests that mechanotaxis can be induced if both the jump in elasticity and the elasticity gradient are sufficiently large.

3.4. Characterization of the distribution of focal adhesions across the elasticity boundary

One of the essential conditions for inducing mechanotaxis as clarified above was a sharp elasticity gradient, where the width of the boundary is comparable to a single cell's adhered size of 50–100 μm. Therefore, we considered that the driving factor of mechanotaxis is related to cell polarity induced across the elasticity boundary. To confirm this polar character of cells adhered across the boundary, the distribution of focal adhesions around the boundary on Gel C was analyzed by immunofluorescently observing the assembly of vinculins. As shown in Fig. 5a in a typical observation, rich lamellipodium

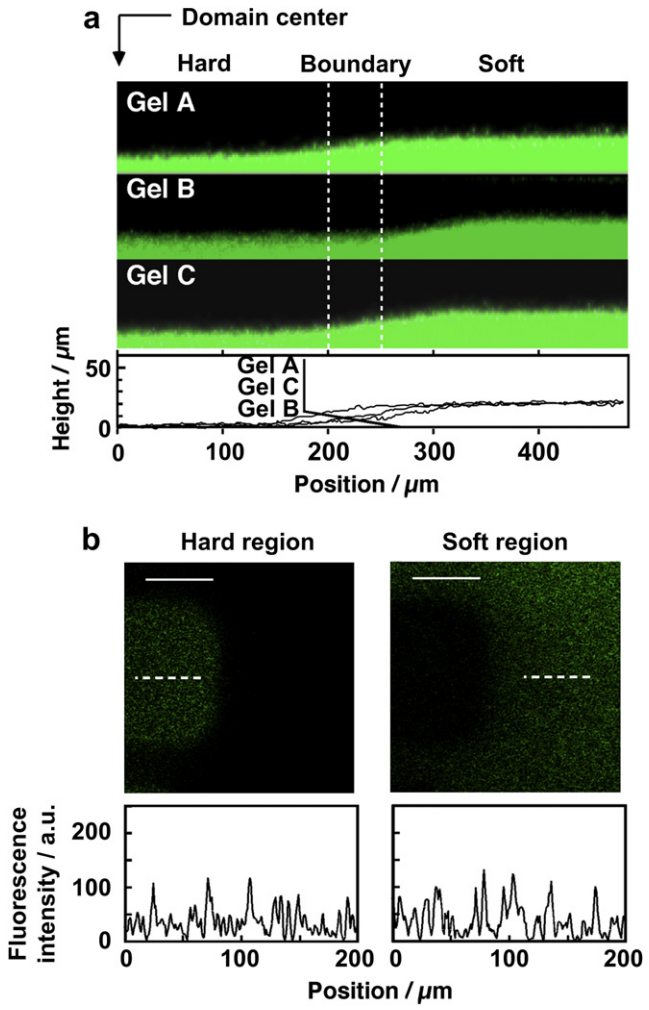

Fig. 2. Characterization of surface topography and adsorption of fibronectin around the microelasticity gradient. a) Confocal microscopic cross-sectional view of the elasticity boundaries in Gels A, B, and C stained by the adsorption of fluorescein-labeled albumin. The positions of the boundary region indicated by the white broken lines were determined based on data in Fig. 1. b) Confocal microscopic images and fluorescence intensity profiles of the top surface of the hard and soft regions in Gel C on which Alexa 488-labeled fibronectin was allowed to adsorb for 24 h. Observations are with a layer 10 μm thick. Scale bar: 200 μm. Fluorescence intensity profiles are plotted along the white broken lines in the upper photos. To extract fluorescence signals only from the top surface of each region, a layer in the upper image was subtracted from the original image which included the region of interest.

and many larger FAs were predominantly formed in the hard region on the left (also see Supplementary Fig. 1). To quantitatively characterize this trend, the number, area and size of FAs were measured by image analysis. The results clearly showed that the number of focal adhesions was asymmetrically distributed across the boundary, indicating that the hard region induced more stable FAs than the soft region (Fig. 5b), and the area and size of each FA were determined to be significantly larger in the harder region (Fig. 5c and d). On Gel C, which induces mechanotaxis, the distribution of FAs across the elasticity boundary was confirmed to be significantly asymmetric, and thus generated significant cell polarity.

4. Discussion

In general, directional cell movement, so-called taxis behavior, is induced by various types of gradients of stimulus intensities or field conditions in the extracellular milieu, which include gradients in the concentration of chemoattractants (driving factor for chemotaxis) [12,13], light intensity (phototaxis) [46], gravity (geotaxis) [47], voltage strength (galvanotaxis) [48], density distribution of haptoattractants (haptotaxis) [28,29], and stiffness (mechanotaxis) [30]. Gradients of these factors induce certain cell polarity through a specific mechanism in each type of taxis. In the case of mechanotaxis, what quantitative conditions regarding the elasticity gradient are required to induce cell polarity?. There have been few previous studies on this aspect of mechanotaxis, and only a few quantitative conditions of the elasticity gradient have been reported. For example, in the first report on the mechanotaxis of fibroblast cells [30], an elasticity gradient was prepared by the simple juxtapositioning of soft (14 kPa) and hard (30 kPa) gels of collagen-coated poly acrylamide (PAAm), and the width of the boundary was 50 μm. The second report described a microelasticity patterning method based on soft-lithography using a PDMS mold, by which mechanotaxis-based fibroblast accumulation was induced in a hard PDMS domain (2.5 MPa) compared with a surrounding softer region (12 kPa) [31]. A series of works by Wong et al. [32,34,35] showed that smooth muscle cells exhibit significant mechanotaxis under an elasticity gradient of 4 kPa/100 μm on collagen-coated PAAm gels [35], which were prepared using a microfluidics-based gradient generator [33]. On the other hand, Cheung et al. reported that an elasticity boundary of ca. 15 kPa/50 μm effectively induces mechanotaxis of fibroblast cells on fibrinogen-functionalized PEG-diacrylate photo-crosslinked gels by microfluidics-based lithography [36]. As seen in this survey of previous findings, the design criteria for the microelasticity gradient needed to induce mechanotaxis are not yet clear, and this is due to the technical difficulty of systematically preparing well-defined elasticity boundaries on a cell-adhesive hydrogel surface under fixed conditions of surface

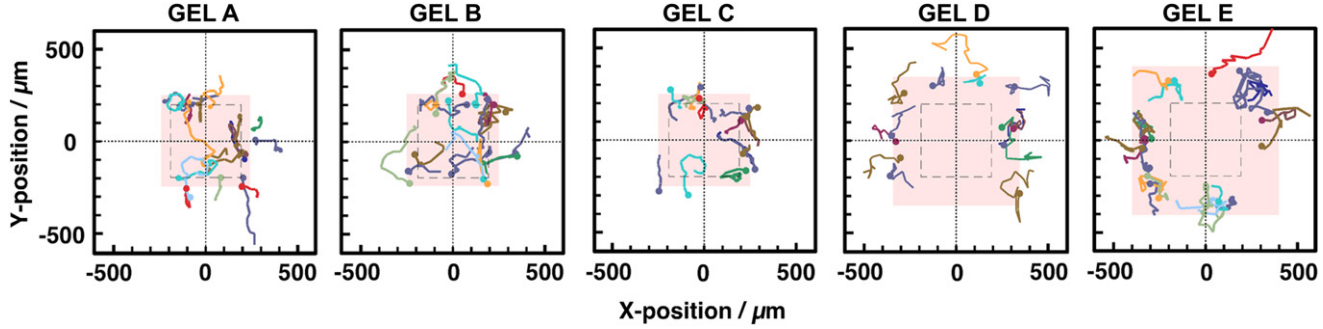

Fig. 3. Raw cell trajectories observed around elasticity boundaries with different gradient conditions. The results for three runs of time-lapse observation every 15 min for 6 h were superimposed. Cell numbers observed: Gel A; $n = 19$. Gel B; $n = 20$. Gel C; $n = 17$. Gel D; $n = 13$. Gel E; $n = 21$. The starting positions of each trajectory are indicated by a dot. The original photomask pattern is indicated by a broken frame, and the resulting hard domains are shown as colored regions with the edge of elasticity defined using data in Fig. 1.

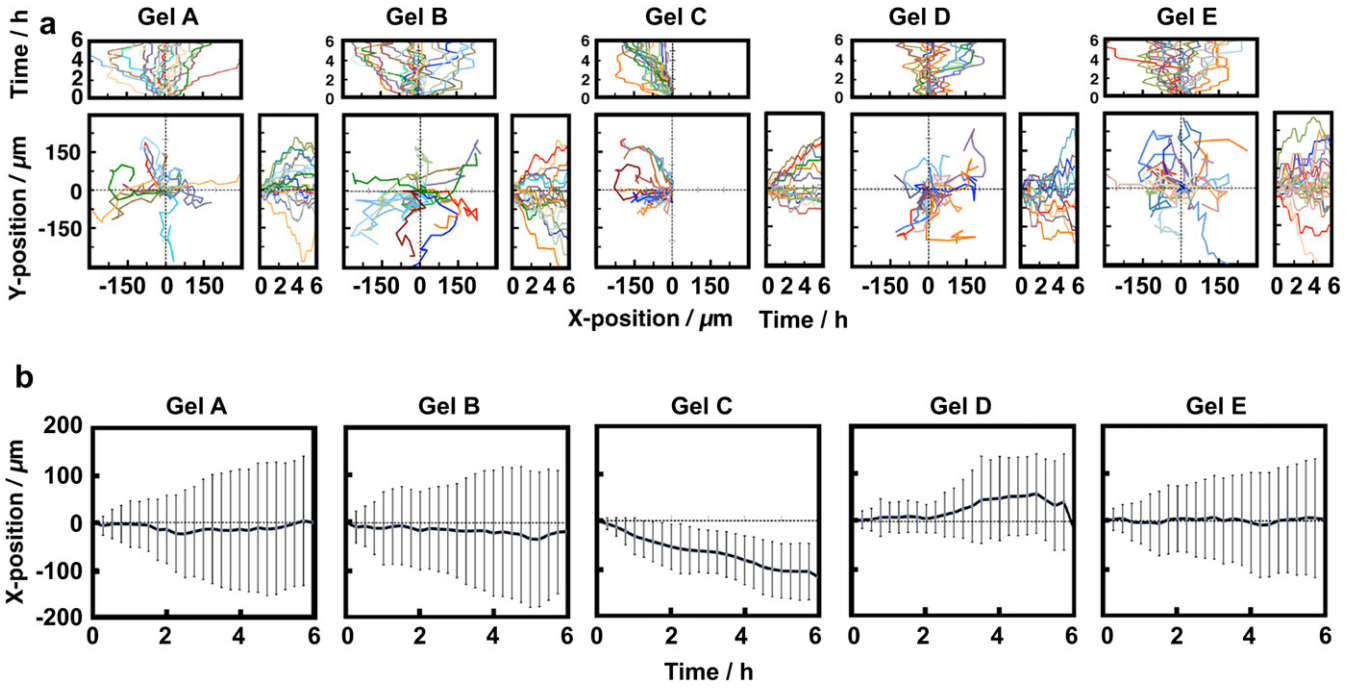

Fig. 4. Transformed presentation of cell trajectories observed in Fig. 3. a) Starting position-superimposed trajectories and time-course trajectories in the *X*- and *Y*-directions. The method used for transformation is described in the text. b) Ensemble-averaged time-course trajectory in the *X*-direction. The *X*-positions of all of the cells observed were averaged and plotted together with their standard deviations.

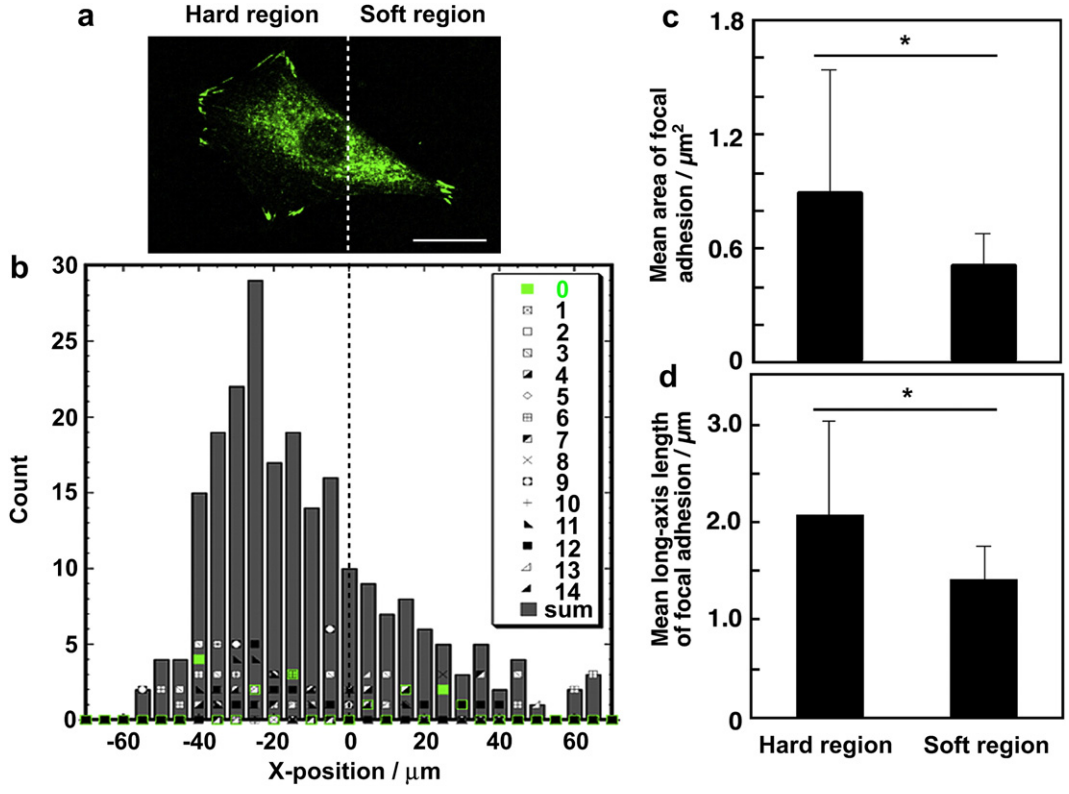

Fig. 5. Characterization of the distribution of focal adhesions across the elasticity boundary. a) Typical confocal microscopic observation of the distribution of focal adhesion in adherent cells across the elasticity boundary on Gel C, visualized with immunofluorescence-labeled vinculins. The boundary position indicated by a white broken line was observed under low magnification in the reflection mode and superimposed in the high-magnification fluorescence observation. Scale bar: 20 μm b) Distribution of the number of focal adhesions in the *X*-direction measured by image analysis for 14 cells adhered across the elasticity boundary. The number of objects larger than 3 pixels obtained after treatment to reduce noise was counted along the *Y*-axis parallel to the elasticity boundary for each *X* position. c) and d): Mean area and mean long-axis length, respectively, of the observed focal adhesions. *Statistically significant level: $P < 0.01$ (*t*-test; numbers of focal adhesion measured in the hard and soft regions were 192 and 53, respectively).

topography and surface chemistry, both of which affect cell motility. In the present study, we tried to clarify the general quantitative design criteria for a microelasticity boundary to induce mechanotaxis by addressing these problems through the use of a photolithographic method with photocurable styrenated gelatins.

The results led to the conclusion that mechanotaxis is induced under a sufficiently high jump in elasticity at a sharp elasticity boundary with a width comparable to a single cell's adhered region. In our 30 wt% StG gel system, the required jump in elasticity was ca. 40 kPa, and the boundary width was determined to be 50 μm (Gel C). Jumps of 3 and 20 kPa with a 50-μm-wide boundary (Gels A and B) did not induce any directional movement. On the other hand, under the conditions for Gels D and E, the jump in elasticity per single cell adhered region (typical long-axis length of cultured fibroblasts is 50–100 μm) can be calculated to be ca. 20 kPa (40 kPa/150 μm × 70 μm) and 10 kPa (40 kPa/250 μm × 70 μm), respectively (mean long-axis length was considered to be 70 μm for simplicity), which did not induce mechanotaxis. These data clearly indicated that a certain threshold jump in elasticity and a narrow width of the elasticity boundary are essential for inducing mechanotaxis, which can also be expressed as the importance of a threshold gradient strength [35]. In our gelatinous gel system, 30–40 kPa/50 μm was required. While a direct comparison of the boundary conditions described in the literature with our data is not appropriate since the absolute values for the elasticity gradient should vary depending on the properties of the gel matrix used, such as kind and density of the component polymers, our findings were similar to those reported by Cheung et al. [36] for fibroblast cells. On the other hand, the gradient strength is much greater than the values observed for smooth muscle cells (4 kPa/100 μm) [35]. This difference in the strength of the elasticity gradient required may be due to the differences in cell types. Cell type-dependent differences in mechanotaxis may be useful for the development of cell-separation materials.

To rigorously characterize mechanotaxis behavior, the following five conditions should be satisfied simultaneously: (1) cell-adhesive hydrogel composed of single-chemical components, (2) tunable surface elasticity, (3) ability to produce a sharp elasticity boundary comparable to the size of a single cell, (4) a constant adsorbed density of cell-adhesive protein regardless of the surface elasticity, and (5) a smooth surface topography around the elasticity boundary. Our photocurable gelatinous gels ensured conditions (1) and (2), and the photolithographic microelasticity patterning method realized condition (3). With regard to condition (4), our system showed an almost constant amount of adsorbed fibronectin between the hard and soft regions, as shown in Fig. 2, which is due to the uniformity of the matrix density of StG gel independent of the crosslinking density. A single molecule of StG polymer has about 30 vinyl groups that can be used for crosslinking. Even under a low degree of crosslinking, if at least one vinyl group is crosslinked, the entire StG polymer should be trapped and not released from the resulting gel matrix, to produce a nearly uniform density matrix. This situation makes the amount of fibronectin adsorbed almost constant. Finally, with regard to condition (5), which involves the issue of surface topography, careful setting of the focus of the photolithographically-projected patterns onto the StG sol is essential. The regular setting of good focus has a rather negative effect on the smooth topographic connection between the hard and soft regions. When the regular setting was used, a hill-and-valley topography was formed and mechanotaxis behavior was completely inhibited. To exclude this negative effect, the focus condition was carefully set. Confirmation of these required conditions suggests that the directional cell migration observed in our system was independent of the effect of surface topography and chemical properties, and therefore it can be attributed to cell-substrate mechanical interaction, which can be characterized as cell mechanotaxis. A photolithographic microelastic patterning method using StG polymer can completely satisfy the above five requirements, and the obtained criteria for the elasticity boundary are the first complete quantitative criteria needed for the induction of mechanotaxis.

With regard to the mechanism of mechanotaxis, under an elasticity gradient that is sufficiently strong to induce mechanotaxis, significant cell polarity was induced across the elasticity boundary, as confirmed by the asymmetric distribution of the numbers and sizes of focal adhesions around the boundary (Fig. 5). This observation suggested that the amount and character of intracellular mechanosignals from the elastic substrate through each focal adhesion site asymmetrically vary across the elasticity boundary in an elasticity-dependent manner. While the details of the molecular transmitting cascade of FA-route mechanosignals [49] are quite complex, a possible mechanism for mechanosignal transmission is outlined below: (1) Substrate elasticity affects the assembling activity of focal adhesion proteins through dynamic mechanical interactions between actin cytoskeletal tension and substrate stress responses, where force-responsive mechanosensory proteins such as FAK [50], p130Cas [51], talin [52], filamin [53], and fibronectin [54], etc. play critical roles to recruit subsequent assembling proteins to the FA site. (2) An increase in the traction force at the FA site resulting from the above process may activate stress-sensitive ion channel, such as Ca^{2+} channel [55,56]. Especially, the amplitude of spontaneous fluctuation in the cytosolic Ca^{2+} concentration has been found to be higher in cells on a hard region than on a softer region [57]. (3) A protein-activating cascade of tyrosine phosphorylation involved in the FA-assembly process and the mechanically-induced inflow of second-messenger ions can regulate the remodeling of cytoskeletal structures, the strength of contractile forces, and the stability of FA, which would determine both static cell morphology and dynamic cell motility. The introduction of a discontinuous elasticity boundary in a single-cell adhered region can lead to asymmetric cell behavior on each region with different elasticities based on these mechanisms. This effect of an elasticity boundary may be an essential driving trigger to produce the asymmetric FA distribution observed in the present study. An elasticity boundary with a systematically well-defined gradient strength should provide an appropriate platform to precisely characterize the quantitative relationship between FA-route mechanosignal input and the driving forces of directional cell motility, and this should enhance our basic understanding of the mechanics of cell motility.

5. Conclusion

In the present study, to establish quantitative design criteria for inducing mechanotaxis, the effects of the boundary conditions of a microelasticity gradient in gelatinous gels were systematically assessed with respect to fibroblast migration. The conditions that were essential for inducing mechanotaxis were a certain threshold jump in elasticity and a sufficiently narrow width of the elasticity boundary, comparable to a single cell's adhered area, i.e., an adequate gradient strength (30–40 kPa/50 μm in our gelatinous gel system). On the other hand, boundary conditions of 3–20 kPa/50 μm did not induce mechanotaxis. A significant asymmetric distribution of focal adhesions across the elasticity boundary was confirmed to be a driving factor for mechanotaxis. The precise and systematic fabrication of a microelasticity boundary is important for controlling mechanotaxis behaviors.

Acknowledgment

This work was supported the following grants: Grants-in-aid for the PRESTO program "Nanosystems and Emergent Functions" from the Japan Science Technology (JST) Agency to S. K, the Scientific

Research on Priority Area “System Cell Engineering”, the Global COE program “Science for Future Molecular Systems”, and the Management Expenses Grants for National Universities Corporations “Nano-Macro Materials, Devices and System Research Alliancefrom” from the Ministry of Education, Culture, Sports, Science and Technology (MEXT) of Japan. The authors sincerely thank Prof. Takehisa Matsuda of Kanazawa Institute of Technology, Japan, for his assistance with the synthesis of styrenated gelatins.

Appendix. Supplementary material

Supplementary data related to this article can be found online at doi:10.1016/j.biomaterials.2011.01.009.

Appendix

Figures with essential colour discrimination. Certain figures in this article, particularly Figs. 2–5 and Scheme 1 are difficult to interpret in black and white. The full colour images can be found in the online version, at doi:10.1016/j.biomaterials.2011.01.009.

References

[1] Juliano RL, Haskill S. Signal transduction from the extracellular matrix. J Cell Biol 1993;120:577–85.
[2] Parente L, Koh MS, Willoughby DA, Kitchen A. Studies on cell motility in inflammation. I. The chemotactic activity of experimental, immunological and non-immunological, inflammatory exudates. Agents Actions 1979;9:190–5.
[3] Parente L, Koh MS, Willoughby DA, Kitchen A. Studies on cell motility in inflammation. II. The in vivo effect of anti-inflammatory and anti-rheumatic drugs on chemotaxis in vitro. Agents Actions 1979;9:196–200.
[4] Martin P. Wound healing: aiming for perfect skin regeneration. Science 1997; 276:75–81.
[5] Berstein LR, Liotta LA. Molecular mediators of interactions with extracellular matrix components in metastasis and angiogenesis. Curr Opin Oncol 1994;6: 106–13.
[6] Orive G, Anitua E, Pedraz JL, Emerich DF. Biomaterials for promoting brain protection, repair and regeneration. Nat Rev Neurosci 2009;10:682–92.
[7] Andrés V. Control of vascular cell proliferation and migration by cyclin-dependent kinase signaling: new perspectives and therapeutic potential. Cardiovasc Res 2004;63:11–21.
[8] Xia Y, Karin M. The control of cell motility and epithelial morphogenesis by Jun kinases. Trends Cell Biol 2004;14:94–101.
[9] Cornwell KG, Downing BR, Brett R, Pins GD. Characterizing fibroblast migration on discrete collagen threads for applications in tissue regeneration. J Biomed Mater Res 2004;71A:55–62.
[10] Ueda-Yukoshi T, Matsuda T. Cellular responses on a wettability gradient surface with continuous variations in surface compositions of carbonate and hydroxyl groups. Langmuir 1995;11:4135–40.
[11] Lee K-W, Wang S, Dadsetan M, Yaszemski MJ, Lu L. Enhanced cell ingrowth and proliferation through three-dimensional nanocomposite scaffolds with controlled pore structures. Biomacromolecules 2010;11:682–9.
[12] Carter SB. Principles of cell motility: the direction of cell movement and cancer invasion. Nature 1965;208:1183–7.
[13] Wilkinson PC. Cell locomotion and chemotaxis: basic concepts and methodological approaches. Methods 1996;10:74–81.
[14] McCarthy JB, Palm SL, Furcht LT. Migration by haptotaxis of Schwann cell tumor line to the basement membrane glycoprotein laminin. J Cell Biol 1983; 97:772–7.
[15] Brandley BK, Schnaar RL. Tumor cell haptotaxis on covalently immobilized linear and exponential gradients of cell adhesion peptide. Dev Biol 1989;135: 74–86.
[16] Rhoads DS, Guan J-L. Analysis of directional cell migration on defined FN gradients: role of intracellular signaling molecules. Exp Cell Res 2007;313: 3859–67.
[17] Tijia JS, Moghe RV. Regulation of cell motility on polymer substrates via “dynamic” cell internalizable, ligand microinterfaces. Tissue Eng 2002;8:247–61.
[18] Leclerc E, Baudoin R, Corlu A, Griscom L, Duval JL, Legallais C. Selective control of liver and kidney cells migration during organotypic cocultures inside fibronectin-coated rectangular silicone microchannels. Biomaterials 2007;28:1820–9.
[19] Anderson EJ, Knothe Take ML. Design of tissue engineering scaffolds as delivery devices for mechanical and mechanically modulated signals. Tissue Eng 2007;13:2525–38.
[20] Nain AS, Phillippi JA, Sitti M, MacKrell J, Campbell PG, Amon C. Control of cell behavior by aligned micr/nanofibrous biomaterial scaffolds fabricated by spinneret-based tunable engineered parameters (STEP) techniques. Small 2008;8:1153–9.
[21] Tayalia P, Mendonca CR, Baldacchini T, Mooney DJ, Mazur E. 3D cell-migration studies using two-photon engineered polymer scaffolds. Adv Mater 2008;20: 4494–8.
[22] Kim D-H, Seo C-H, Han K, Kwon KW, Levchenko A, Suh K-Y. Guided cell migration on micropatterned substrates with variable local density and anisotropy. Adv Funct Mater 2009;19:1579–86.
[23] Frey M, Wang Y-L. A photo-modulatable material for probing cellular responses to substrate rigidity. Soft Matter 2009;5:1918–24.
[24] Kim D-H, Han K, Gupta K, Kwon KW, Suh K-Y, Levchenko A. Mechanosensitivity of fibroblast cell shape and movement to anisotropic substratum topography gradients. Biomaterials 2009;30:5433–44.
[25] Nemir S, Hayenga HN, West JL. PEGDA hydogels with patterned elasticity: novel tools for the study of cell responses to substrate rigidity. Biotechnol Bioeng 2010;105:636–44.
[26] Weiss P. The problem of specificity in growth and development. Yale J Biol Med 1945;19:239–78.
[27] Weiss P. Cell contact. Int Rev Cytol 1985;7:391–423.
[28] Carter SB. Haptotaxis and the mechanism of cell motility. Nature 1967;213: 256–60.
[29] Jung DR, Kapur R, Adams T, Giuliano KA, Mrksich M, Craighead HG, et al. Topographical and physicochemical modification of material surface to enable patterning of living cells. Crit Rev Biotechnol 2001;21:111–54.
[30] Lo C-M, Wang H-B, Dembo M, Wang Y-L. Cell movement is guided by rigidity of the substrate. Biophys J 2000;79:141–52.
[31] Gray DS, Tien J, Chen CS. Repositioning of cells by mechanotaxis on surfaces with micropattened Young's modulus. J Biomed Mater Res 2003;66A:605–14.
[32] Wong JY, Velasco A, Rajagopalan P, Pham Q. Directed movement of vascular smooth muscle cells on gradient-compliant hydogels. Langmuir 2003;19: 1908–13.
[33] Burdick JA, Khademhosseini A, Langer R. Fabrication of gradient hydrogels using a microfluidics/photopolymerization process. Langmuir 2004;20:5153–6.
[34] Zaari N, Rajagopalam P, Kim SK, Engler AJ, Wong JY. Photopolymerization in microfluidics gradient generators: microscale gradient of substrate compliance to manipulate cell response. Adv Mater 2004;16:2133–7.
[35] Isenberg BC, Dimilla PA, Walker M, Kim S, Wong JY. Vascular smooth muscle cell durotaxis depends on substrate stiffness gradient strength. Biophys J 2009;97:1313–22.
[36] Cheung YK, Azeloglu EU, Shiovitz DA, Costa KD, Seliktar D, Sia SK. Microscale control of stiffness in a cell-adhesive substrate using microfluidics-based lithography. Angew Chem Int Ed 2009;48:1–6.
[37] Hadjipanayi E, Mudera V, Brown RA. Guiding cell migration in 3D: a collagen matrix with graded directional stiffness. Cell Motil Cytoskeleton 2009; 66:121–8.
[38] Hale NA, Yang Y, Rajagopalan P. Cell migration at the interface of dual chemical-mechanical gradient. ACS Appl Mater Interfaces 2010;2:2317–24.
[39] Hahn MS, Miller JS, West JL. Three-dimensional biochemical and biomechanical patterning of hydrogels for guiding cell behabiors. Adv Mater 2006; 18:2679–84.
[40] Nemir S, Hayenga HN, West JL. PEGDA hydrogels with patterned elasticity: novel tools for the study of cell responses to substrate rigidity. Biotechnol Bioeng 2009;105:636–44.
[41] Kidoaki S, Matsuda T. Microelastic gradient gelatinous gels to induce cellular mechanotaxis. J Biotechnol 2008;133:225–30.
[42] Okino H, Nakayama Y, Tanaka M, Matsuda T. *In situ* hydrogelation of photocurable gelatin and drug release. J Biomed Mater Res 2002;59:233–45.
[43] Hertz H. Ueber die Beruhrrung fester elastischer Korper. J Reine Angew Mathematik 1881;92:156–71.
[44] Sneddon IN. The relation between load and penetration in the axisymmetric Boussinesq problem for a punch of arbitrary profile. Int J Eng Sci 1965; 3:47–57.
[45] Weisenhorn AL, Khorsandi M, Kasas S, Gotzos V, Butt H-J. Deformation and height anomaly of soft surfaces studied with an AFM. Nanotechnology 1993; 4:106–13.
[46] Saranak J, Foster KW. Rhodopsin guides fungal phototaxis. Nature 1997; 387:465–6.
[47] Lowe B. The role of Ca^{2+} in deflection-induced excitation of motile, mechanoresponsive balancer cilia in the ctenophore statocyst. J Exp Biol 1997; 200:1593–606.
[48] Erickson CA, Nuccitelli R. Embryonic fibroblast motility and orientation can be influenced by physiological electric fields. J Cell Biol 1984;98:296–307.
[49] Moore SW, Roca-Cusachs P, Sheetz MP. Stretchy proteins on stretchy substrates: the important elements of integrin-mediated rigidity sensing. Dev Cell 2010;19:194–206.
[50] Cooper LA, Shen TL, Guan JL. Regulation of focal adhesion kinase by its amino-terminal domain through an autoinhibitory interaction. Mol Cell Biol 2003;23:8030–41.
[51] Sawada Y, Tamada M, Dubin-Thaler BJ, Cherniavskaya O, Sakai R, Tanaka S, et al. Force sensing by mechanical extension of the Src family kinase substrate p130Cas. Cell 2006;127:1015–26.
[52] del Rio A, Perez-Jimenez R, Liu R, Roca-Cusachs P, Fernandez JM, Sheetz MP. Stretching single talin rod molecules activates vinculin binding. Science 2009;323:638–41.
[53] Furuike S, Ito T, Yamazaki M. Mechanical unfolding of single filamin A (ABP-280) molecules detected by atomic force microscopy. FEBS Lett 2001; 498:72–5.

[54] Vogel V. Mechanotransduction involving multimodular proteins: converting force into biochemical signals. Annu Rev Biophys Biomol Struct 2006;35:459–88.
[55] Munevar S, Wang Y-L, Dembo M. Regulation of mechanical interactions between fibroblasts and the substratum by stretch-activated Ca^{2+} entry. J Cell Sci 2003;117:85–92.
[56] Hayakawa K, Tatsumi H, Sokabe M. Actin stress fibers transmit and focus force to activate mechanosensitive channels. J Cell Sci 2008;121:496–503.
[57] Kobayashi T, Sokabe M. Sensing substrate rigidity by mechanosensitive ion channels with stress fibers and focal adhesions. Curr Opin Cell Biol 2010; 22:1–8.